doi:10.1038/nature08944

LETTERS

The kinetics of two-dimensional TCR and pMHC interactions determine T-cell responsiveness

Jun Huang[1]†, Veronika I. Zarnitsyna[1], Baoyu Liu[1], Lindsay J. Edwards[2], Ning Jiang[1]†, Brian D. Evavold[2] & Cheng Zhu[1]

The T-cell receptor (TCR) interacts with peptide-major histocompatibility complexes (pMHC) to discriminate pathogens from self-antigens and trigger adaptive immune responses. Direct physical contact is required between the T cell and the antigen-presenting cell for cross-junctional binding where the TCR and pMHC are anchored on two-dimensional (2D) membranes of the apposing cells[1]. Despite their 2D nature, TCR–pMHC binding kinetics have only been analysed three-dimensionally (3D) with a varying degree of correlation with the T-cell responsiveness[2–4]. Here we use two mechanical assays[5,6] to show high 2D affinities between a TCR and its antigenic pMHC driven by rapid on-rates. Compared to their 3D counterparts, 2D affinities and on-rates of the TCR for a panel of pMHC ligands possess far broader dynamic ranges that match that of their corresponding T-cell responses. The best 3D predictor of response is the off-rate, with agonist pMHC dissociating the slowest[2–4]. In contrast, 2D off-rates are up to 8,300-fold faster, with the agonist pMHC dissociating the fastest. Our 2D data suggest rapid antigen sampling by T cells and serial engagement of a few agonist pMHCs by TCRs in a large self pMHC background. Thus, the cellular environment amplifies the intrinsic TCR–pMHC binding to generate broad affinities and rapid kinetics that determine T-cell responsiveness.

The sustained interest in the kinetic analysis of TCR–pMHC interactions stems from a fundamental hypothesis that the interaction parameters have a central role in determining the subsequent T-cell response. We analysed 2D TCR–pMHC interactions on naive $CD8^+$ OT1 T cells with the adhesion frequency[5,7] and thermal fluctuation[6,8] assays using a micropipette (Fig. 1a) and a biomembrane force probe (BFP, Fig. 1b). Both use a red blood cell (RBC) as an adhesion sensor, but the BFP also attaches a bead to the RBC. The RBC or bead was functionalized with pMHC mutated to abrogate CD8 binding[9] (Fig. 1c and Methods).

In the adhesion frequency assay[5,7], a T cell (Fig. 1a, b, right) was micro-manipulated to touch the RBC or bead with a controlled contact area and time. TCR–pMHC binding (if present) was observed visually by RBC elongation (Supplementary Movie 1) or detected by the bead displacement (Supplementary Movie 2) on T-cell retraction. To determine the likelihood of adhesion, the cell pair was repeatedly moved in and out of contact for a given contact time (t_c) to yield an adhesion frequency (P_a)—that is, the number of adhesions divided by the number of total contacts. The adhesion frequencies were specific because binding was abolished unless OT1 TCR and antigenic pMHC were used (Fig. 1d). Using a divalent streptavidin[10] to ensure monomeric pMHC presentation (Fig. 1c) produced a similar adhesion frequency as using a tetravalent wild-type streptavidin to couple pMHC on RBCs (Fig. 1e), ruling out multimeric pMHC as the cause for high affinity binding (see later).

The 2D kinetic information is extracted by fitting an adhesion frequency curve measured using many cell pairs over a range of contact times with a mathematical model[5] (Fig. 2a–c), which derives separately two parameters ($m_r m_l A_c K_a$ and k_{off}) with good accuracy (Methods and Supplementary Fig. 1). The 2D affinity K_a has a unit of area rather than volume—the unit of 3D affinity. We report the effective 2D affinity ($A_c K_a$, in μm^4) as it is evaluated together with the contact area A_c (a few per cent of 3 μm^2 for micropipette or of 1 μm^2 for BFP). Adhesion frequency depends on the receptor (m_r) and ligand (m_l) densities. For example, three different ovalbumin (OVA) pMHC densities yielded three distinct adhesion levels (Fig. 2a) but the same affinity is derived (Supplementary Fig. 2). The weaker ligands R4 (Fig. 2b) and G4 (Fig. 2c) required higher densities than OVA (Fig. 2a, c) yet still generated lower adhesion levels, indicating far lower affinities. The 2D off-rate k_{off} is not affected by the contact area or protein densities and is inversely proportional to the time $t_{1/2}$ required to reach a half-maximal P_a level[5] (Methods). The OVA curves in Fig. 2a reached equilibrium very rapidly, indicating a fast off-rate that required the BFP to measure accurately (Fig. 2c). The R4 (Fig. 2b) and G4 (Fig. 2c) curves rose more slowly, indicating slower off-rates. The effective 2D on-rate $A_c k_{on}$ ($= A_c K_a \times k_{off}$) equals the initial slope of the adhesion curve divided by the receptor and ligand densities. The much steeper initial slopes yet lower pMHC densities of the adhesion curves for OVA (Fig. 2a, c) compared to R4 (Fig. 2b) and G4 (Fig. 2c) indicate a much faster association of TCR with OVA.

In the thermal fluctuation assay[6,8] (Methods), association/dissociation events of TCR–pMHC bonds were identified by reduction/resumption of thermal fluctuations of the BFP bead because bond formation anchored the bead to the T cell, restricting its movements (Supplementary Fig. 3 and Supplementary Movie 3). The time from association to dissociation is bond lifetime t_b, the distributions of which line up in semi-log plots that linearize exponential decays, suggesting first-order dissociation of single-bonds for both OVA and G4 (Fig. 2d). Their respective off-rates equal the negative slope of the lines (Fig. 2d), which agree with the corresponding values from the adhesion curves (Fig. 2c). These results confirm that both assays measure stress-free kinetics despite the use of force to break any bond present at the end of each contact cycle[5–8].

We compared 2D parameters of the OT1 TCR binding to a panel of pMHCs with increasing potencies[3] to the published 3D results[11,12] (Fig. 3). Regardless of receptor and ligand densities, the same monomeric binding model[5] fits adhesion curves at both 25 and 37 °C equally well for all ligands (Supplementary Fig. 2), with higher temperature yielding higher affinities (Table 1). The effective 2D affinities from antagonist to agonist pMHC spanned three logs from 10^{-6} to 10^{-3} μm^4, whereas that of null (vesicular stomatitis virus, or VSV)

[1]Coulter Department of Biomedical Engineering, Georgia Institute of Technology, Atlanta, Georgia 30332, USA. [2]Department of Microbiology and Immunology, Emory University School of Medicine, Atlanta, Georgia 30322, USA. †Present addresses: Department of Microbiology and Immunology and The Howard Hughes Medical Institute, Stanford University School of Medicine, Stanford, California 94305, USA (J.H.); Department of Bioengineering, Stanford University, Stanford, California 94305, USA (N.J.).

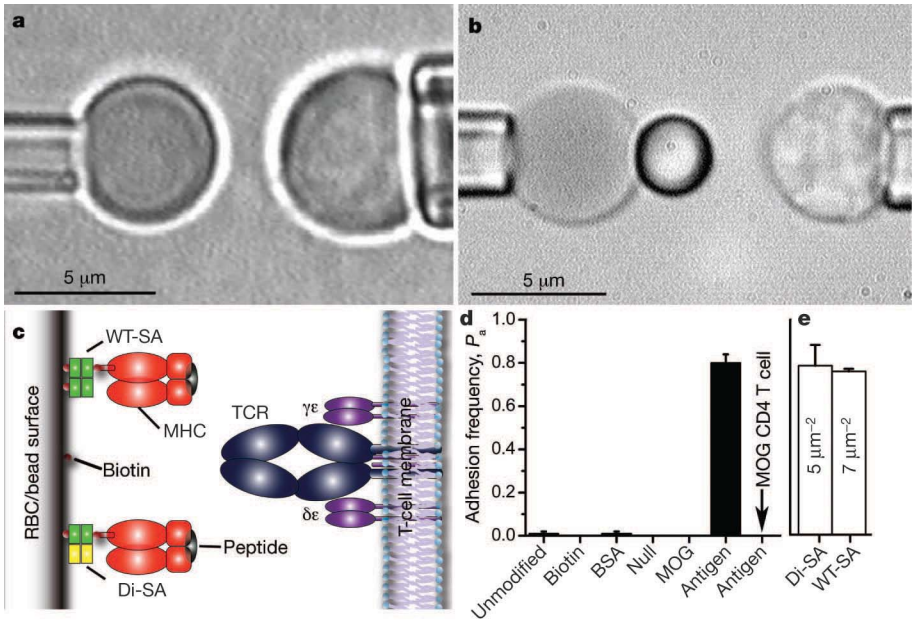

Figure 1 | Micropipette and BFP. **a**, **b**, Micrographs of the micropipette (**a**) and BFP (**b**). A T cell (right) aspirated by a pipette was aligned with a RBC held stationary by another pipette (left) without (**a**, Supplementary Movie 1) or with (**b**, Supplementary Movies 2 and 3) a bead attached to the apex. **c**, RBCs or beads (left) were coupled by wild-type streptavidin (WT-SA) or divalent streptavidin (Di-SA)[10] with monomeric pMHC to interact with the TCR on T cells (right). **d**, Specificity controls of adhesion frequency measured at 5 s between OT1 T cells and unmodified RBCs, biotinylated RBCs without coating, biotinylated RBCs coated with BSA, null pMHC-I (VSV–H-2K^b), pMHC-II (MOG–I-A^b), or antigenic pMHC-I (OVA–H-2K^b), or between MOG CD4$^+$ T cells and biotinylated RBCs coated with OVA–H-2K^b. **e**, Comparison between adhesion frequencies measured at 2 s using 7 and 5 μm^{-2} OVA pMHC, captured by WT-SA and Di-SA, respectively. Each T cell–RBC pair was tested repeatedly for 50 contact cycles to estimate an adhesion frequency, and 3–5 cell pairs were tested for each condition to calculate a mean $P_a \pm$ s.e.m. for data in **d** and **e**.

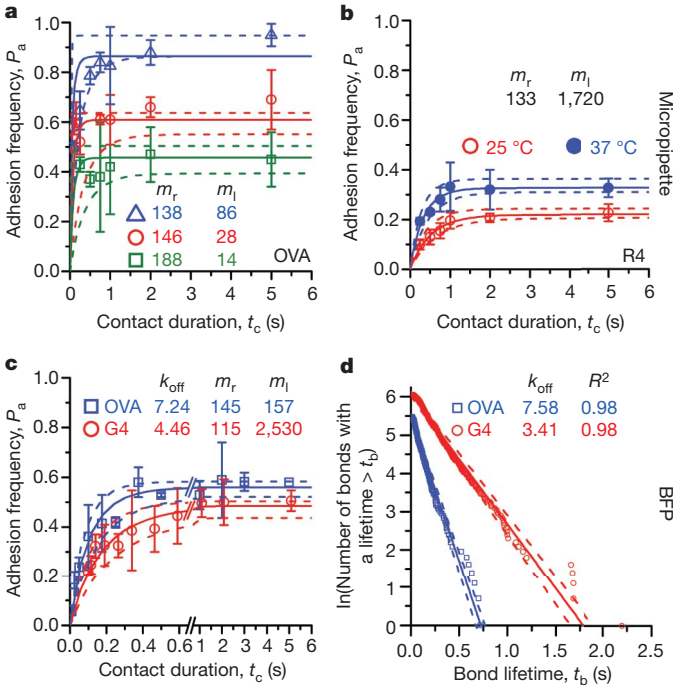

Figure 2 | 2D kinetics measurements. **a**, **b**, Adhesion curves for the OT1 TCR interacting with OVA (**a**) and R4 (**b**) pMHC measured by micropipette at 25 °C (**a**) or both 25 and 37 °C (**b**) at indicated site densities. **c**, Adhesion curves of the OT1 TCR interacting with OVA and G4 pMHC measured by BFP at 25 °C. Each cell pair was tested repeatedly at given contact duration t_c to estimate an adhesion frequency P_a, and 3–5 cell pairs were tested for each t_c to calculate a mean $P_a \pm$ s.e.m. The data (points) were fitted (colour-matched solid curves) by a model for 2D binding kinetics[5] (**a**–**c**). **d**, Pooled ensembles of 239 (OVA, squares) or 424 (G4, circles) lifetimes of OT1 TCR–pMHC bonds were respectively sorted according to their durations. For each pMHC, the natural log of the number of events with a lifetime $\geq t_b$ was plotted against t_b and fitted by a straight line. The negative slope represents off-rate k_{off} (indicated). The goodness-of-fit was indicated by the R^2 values. Colour-matched dotted curves represent 95% confidence intervals of the best-fit curves obtaining by bootstrapping.

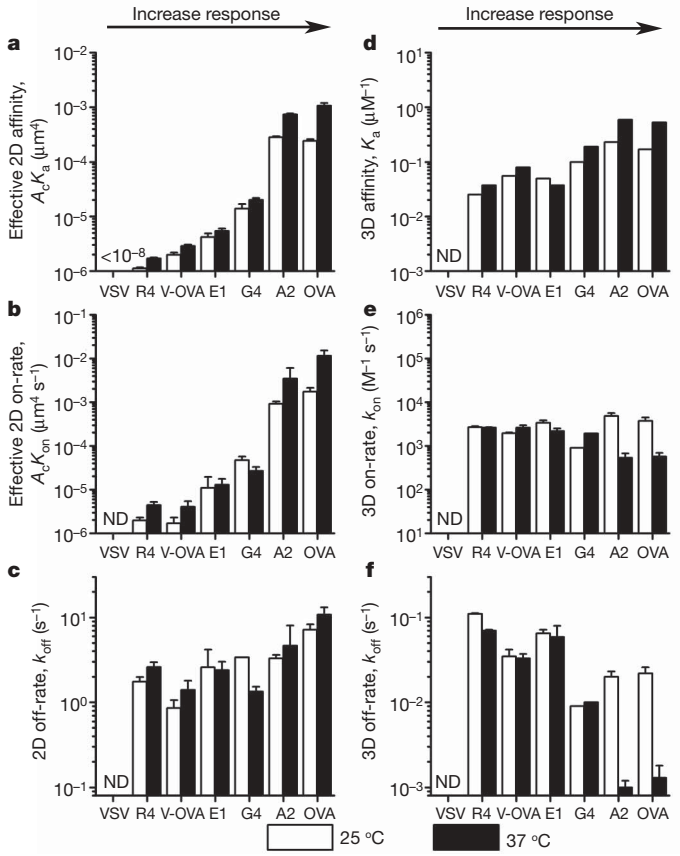

Figure 3 | Comparison of 2D and 3D kinetics. **a**–**f**, Affinities (**a**, **d**), on-rates (**b**, **e**) and off-rates (**c**, **f**) of the OT1 TCR interacting with indicated pMHCs. The 2D data (**a**–**c**) were measured by the adhesion frequency assay and analysed with a monomeric binding model. The 3D data (**d**–**f**) from refs 11 and 12 were measured by surface plasmon resonance and analysed with a monomeric binding model except for the OVA and A2 data at 37 °C, which were analysed with a dimeric binding model (values of the second-step kinetics were plotted). Data are presented as mean ± s.e.m. of parameters evaluated from different adhesion curves measured using different pMHC densities (see Supplementary Fig. 2).

Table 1 | 2D kinetics and binding affinities of OT1 TCR–pMHC interactions

Peptide	Sequence	T-cell activation	$A_c k_{on}$ ($\mu m^4 s^{-1}$)		k_{off} (s^{-1})		$A_c K_a$ (μm^4)	
			25 °C	37 °C	25 °C	37 °C	25 °C	37 °C
OVA	SIINFEKL	Antigen	1.7 ± 0.4 ($\times 10^{-3}$)	1.2 ± 0.4 ($\times 10^{-2}$)	7.2 ± 1.1	10.8 ± 2.3	2.4 ± 0.2 ($\times 10^{-4}$)	1.1 ± 0.1 ($\times 10^{-3}$)
A2	SAINFEKL	Agonist	9.2 ± 1.2 ($\times 10^{-4}$)	3.5 ± 2.6 ($\times 10^{-3}$)	3.3 ± 0.3	4.7 ± 3.4	2.8 ± 0.1 ($\times 10^{-4}$)	7.4 ± 0.3 ($\times 10^{-4}$)
G4	SIIGFEKL	Weak ag. /antag.	4.7 ± 1.0 ($\times 10^{-5}$)	2.7 ± 0.6 ($\times 10^{-5}$)	3.4 ± 0.0	1.3 ± 0.2	1.4 ± 0.3 ($\times 10^{-5}$)	2.0 ± 0.2 ($\times 10^{-5}$)
E1	EIINFEKL	Weak ag. /antag.	1.1 ± 0.9 ($\times 10^{-5}$)	1.3 ± 0.5 ($\times 10^{-5}$)	2.6 ± 1.6	2.4 ± 0.6	4.2 ± 0.7 ($\times 10^{-6}$)	5.4 ± 0.6 ($\times 10^{-6}$)
V-OVA	RGYNYEKY	Antagonist	1.7 ± 0.6 ($\times 10^{-6}$)	4.0 ± 1.4 ($\times 10^{-6}$)	0.9 ± 0.2	1.4 ± 0.4	2.0 ± 0.2 ($\times 10^{-6}$)	2.9 ± 0.2 ($\times 10^{-6}$)
R4	SIIRFEKL	Antagonist	2.0 ± 0.3 ($\times 10^{-6}$)	4.4 ± 0.8 ($\times 10^{-6}$)	1.8 ± 0.2	2.6 ± 0.4	1.1 ± 0.1 ($\times 10^{-6}$)	1.7 ± 0.1 ($\times 10^{-6}$)
VSV	RGYVYQGL	Null	ND	ND	ND	ND	$<10^{-8}$	$<10^{-8}$

ag., agonist; antag., antagonist; ND, not detectable.

pMHC was less than the assay's detection limit[7] of 10^{-8} μm^4 (Fig. 3a). In sharp contrast, the 3D affinities differ by only one log for the same ligand set (Fig. 3d), making them difficult to resolve ligand potencies. Furthermore, the micromolar 3D equilibrium dissociation constant (K_d) conveys the impression that TCR–pMHC binding is of low affinity; however, the OT1 (and F5, Supplementary Fig. 4) TCR on naive (and activated, Supplementary Fig. 5) T cells have effective 2D affinities for agonist pMHCs that are similar to that of high affinity lymphocyte function-associated antigen (LFA)-1 for intercellular adhesion molecule (ICAM)-1 (ref. 13), an interaction that provides strong adhesion for many immune functions.

The high 2D affinities of TCR for agonist pMHCs were driven by rapid 2D on-rates, which were even faster than that of P-selectin associating with P-selectin glycoprotein ligand (PSGL)-1 (ref. 14), an interaction that requires a rapid on-rate to capture flowing leukocytes to inflamed vascular surfaces. Unlike the P-selectin–PSGL-1 interaction, however, the fast 2D on-rates for TCR–pMHC do not translate to fast 3D on-rates. In fact, the 3D TCR–pMHC on-rates[11,12] are >200-fold slower than the P-selectin–PSGL-1 3D on-rate[15]. The 3D TCR–pMHC on-rates are insensitive to the different peptides (Fig. 3e), suggesting that TCR binding is initiated by MHC contact[16]. By comparison, the 2D on-rates spanned four logs for the same ligand set (Fig. 3b), indicating the critical contribution of peptide contact to TCR–pMHC association. Thus, an important attribute of our measurements is their high sensitivity to discriminate binding kinetics for a range of closely related ligands.

The 2D off-rates (Fig. 3c) were 30–8,300-fold faster than the corresponding 3D off-rates (Fig. 3f), with the value for TCR dissociating from OVA–H-2K^b (7.2 and 10.8 s^{-1} at 25 and 37 °C, respectively) comparable to that for L-selectin dissociating from PSGL-1 (10.2 s^{-1} at 25 °C), the most rapid selectin–ligand off-rate in both 2D and 3D, which is required for mediating fast rolling of leukocytes on vascular surfaces[6,17]. Again, the fast 2D off-rates for TCR–pMHC did not translate to fast 3D off-rates. In fact, OVA–H-2K^b dissociates from the OT1 TCR in a single step at 25 °C, with a 3D off-rate of 0.022 s^{-1} but in two steps (that is, requiring dimer formation) at 37 °C, with a 3D off-rate of 0.0012 s^{-1} for the second step[11,12]. Notably, the off-rates of stronger ligands are progressively faster in 2D but slower in 3D, showing opposite trends (compare Fig. 3c and f). Thus, the TCR–pMHC off-rates and their relationships to ligand potency differ substantially between 2D and 3D.

To test further the hypothesis that 2D TCR–pMHC kinetics determines T-cell responsiveness, we measured the peptide concentration required to stimulate half-maximal T-cell proliferation (EC_{50}) and plotted it against the 2D TCR binding parameters measured at 25 °C (Fig. 4a–c) and 37 °C (Fig. 4d–f). A strong correlation was found between $1/EC_{50}$ values and all metrics of 2D kinetics, especially the affinities and on-rates, for their broad dynamic ranges better match the wide range of functional responses. This is, to our knowledge, the first demonstration of the relevance of 2D TCR–pMHC binding kinetics to the functional response of T cells[18]. Besides T-cell proliferation, a late-stage response assessed after 3 days of antigen-presenting cell (APC) stimulation, the more proximal TCR downregulation response used in

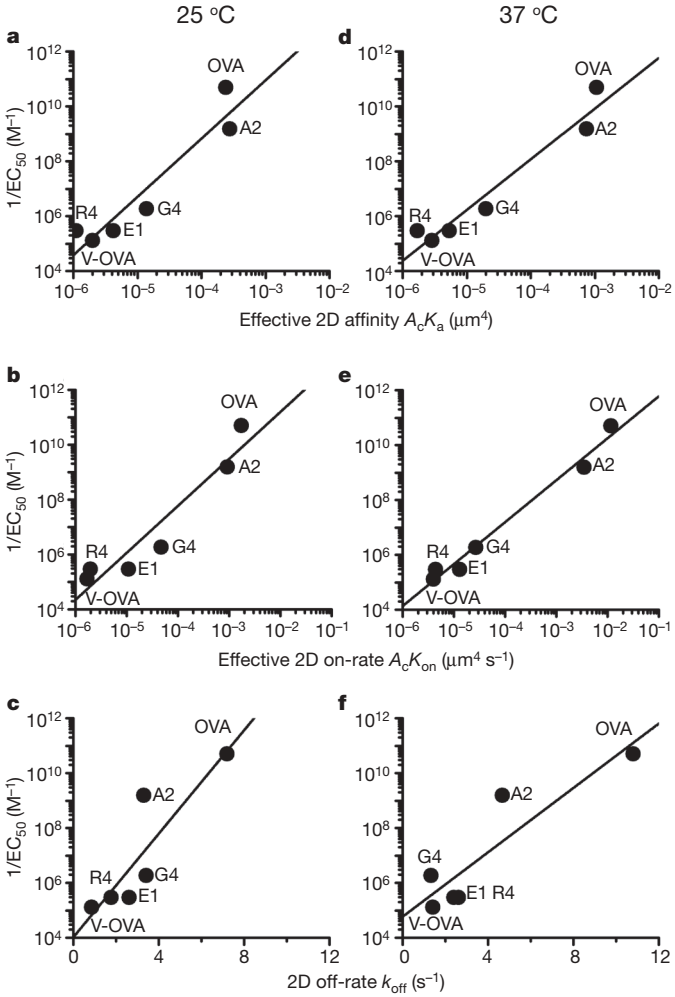

Figure 4 | Correlation between 2D kinetics and T-cell proliferation. **a–f**, The reciprocal concentration required to reach half-maximal T-cell proliferation ($1/EC_{50}$) is plotted against the effective 2D affinity (**a**, **d**), on-rate (**b**, **e**) and off-rate (**c**, **f**) measured at 25 °C (**a–c**) or 37 °C (**d–f**) of the OT1 TCR interacting with the indicated pMHCs. To quantify T-cell proliferation, naive OT1 splenocytes (3×10^5 per well) were cultured in 96-well plates with the indicated peptides at 37 °C. After 48 h, 0.4 μCi per well of [^{3}H]-thymidine was added. After another 18 h, cells were collected on a FilterMate harvester (PerkinElmer) and analysed on a Matrix 96 Direct Beta Counter (PerkinElmer). EC_{50} values were calculated using GraphPad Prism.

a previous 3D study[3] also correlated well with our 2D parameters (Supplementary Fig. 6).

The substantial differences between 2D and 3D kinetics for TCR–pMHC interactions are not seen in ligand binding of selectins and integrins. In light of the recent reports of TCR clustering on the cell surface in a cholesterol- and/or actin cytoskeleton-dependent fashion[19–22], we speculate that the T cell imposes unique regulations on TCR organization, orientation and/or conformation, which may affect the availability of TCR to binding or enable cooperative binding. Although the 3D assays of purified molecules may measure their intrinsic kinetics independent of these regulatory mechanisms, our 2D assays may capture the effect of the cellular environment on TCR–pMHC interactions, which mimics the physiological situation (Supplementary Fig. 7). Consistent with this view, we observed reduced effective 2D affinities of the OT1 TCR for OVA and G4 pMHCs by treatment with methyl-β-cyclodextrin, a water-soluble cyclic heptasaccharide that can extract cholesterol from the plasma membrane[23] and alter TCR preclustered structures[21] (Supplementary Fig. 8). Similar effects were observed by treatment with cholesterol oxidase, another cholesterol depletion agent (Supplementary Fig. 9). Furthermore, the 2D affinities were also reduced by latrunculin A, an inhibitor of actin polymerization (Supplementary Fig. 10). Moreover, Monte Carlo simulations showed an increase in apparent affinity by cooperative binding if it is assumed that the interaction of a pMHC with one TCR in a cluster increases the binding propensity of all members of the TCR cluster (Supplementary Fig. 11). This form of cooperation is suggested by the observed memory effects of TCR–pMHC interactions, such that adhesion in a past contact increases the likelihood of adhesion in the next contact[9].

The insufficient resolution of T-cell responsiveness by 3D TCR–pMHC kinetics (for example, Fig. 3d–f) has generated numerous models to explain the various functional outcomes[2–4,12,18,24–28]. The kinetic proofreading model proposed a serial scheme to amplify the small differences in the 3D TCR–pMHC off-rates[26]. Our data indicate that such amplifications may be integrated into direct measurements on the T-cell membrane as they result in 2D on-rates, off-rates and affinities that all match the T-cell responses to a given set of pMHCs. The broad affinities and rapid kinetics of the 2D interactions meet the requirement for the T cell to scan with high speed and sensitivity the numerous self pMHCs on an APC to find, engage and respond to antigens expressed at low numbers[29]. The observations of antigen sampling by a T cell from several APCs[30] and the rapid microcluster formation between TCR and agonist pMHC further enforce how quickly the pMHC is interrogated to accumulate threshold signalling levels[21,22]. Microclusters of TCR coupled to its rapid 2D kinetics also allow a single pMHC to serially engage many TCRs in a short time. Note that here the term is used differently from the original model in which serial engagement led to TCR internalization[27]. Although the lifetimes of individual TCR–pMHC bonds are brief because they dissociates rapidly, bonds also reform rapidly and frequently because of the fast on-rate. Serial engagement allows both the quality and quantity of pMHCs to be measured by the frequency of bond formation as it is proportional to the 2D affinity and the pMHC density. High bond formation frequency also accumulates a large fraction of engagement time. TCR clustering and cooperative binding could amplify serial engagement as it provides a high local concentration of TCRs, thereby generating maximal recognition signal to trigger downstream events for T-cell activation. Thus, our 2D TCR–pMHC kinetic data may provide a basis for a comprehensive model to explain self/non-self recognition, ligand discrimination, thymocyte selection, signal accumulation, feedback mechanisms, and TCR antagonism.

METHODS SUMMARY

We used adhesion frequency assay[5] and thermal fluctuation assay[6] to measure the 2D kinetics of TCR–pMHC interaction on the cell membrane. The adhesion frequency assay used a micropipette and a BFP, and the thermal fluctuation assay used a BFP. T cells expressing monoclonal OTI or F5 TCR were purified from transgenic mice. Human RBCs directly (or indirectly through a glass bead) coated with pMHC by biotin–streptavidin coupling served as both a surrogate APC and a force sensor for detecting the TCR–pMHC interaction. The site densities of TCR and pMHC were measured by flow cytometry[7]. Monte Carlo simulations and pharmacological treatments were performed to study the effects of T-cell membrane environment on 2D TCR–pMHC binding.

Full Methods and any associated references are available in the online version of the paper at www.nature.com/nature.

Received 5 January; accepted 25 February 2010.
Published online 31 March 2010.

1. Dustin, M. L., Bromley, S. K., Davis, M. M. & Zhu, C. Identification of self through two-dimensional chemistry and synapses. *Annu. Rev. Cell Dev. Biol.* **17,** 133–157 (2001).
2. Davis, M. M. *et al.* Ligand recognition by αβ T cell receptors. *Annu. Rev. Immunol.* **16,** 523–544 (1998).
3. Gascoigne, N. R., Zal, T. & Alam, S. M. T-cell receptor binding kinetics in T-cell development and activation. *Expert Rev. Mol. Med.* **2001,** 1–17 (2001).
4. Stone, J. D., Chervin, A. S. & Kranz, D. M. T-cell receptor binding affinities and kinetics: impact on T-cell activity and specificity. *Immunology* **126,** 165–176 (2009).
5. Chesla, S. E., Selvaraj, P. & Zhu, C. Measuring two-dimensional receptor-ligand binding kinetics by micropipette. *Biophys. J.* **75,** 1553–1572 (1998).
6. Chen, W., Evans, E. A., McEver, R. P. & Zhu, C. Monitoring receptor-ligand interactions between surfaces by thermal fluctuations. *Biophys. J.* **94,** 694–701 (2008).
7. Huang, J., Edwards, L. J., Evavold, B. D. & Zhu, C. Kinetics of MHC-CD8 interaction at the T cell membrane. *J. Immunol.* **179,** 7653–7662 (2007).
8. Chen, W., Zarnitsyna, V. I., Sarangapani, K. K., Huang, J. & Zhu, C. Measuring receptor-ligand binding kinetics on cell surfaces: from adhesion frequency to thermal fluctuation methods. *Cell. Mol. Bioeng.* **1,** 276–288 (2008).
9. Zarnitsyna, V. I. *et al.* Memory in receptor-ligand-mediated cell adhesion. *Proc. Natl Acad. Sci. USA* **104,** 18037–18042 (2007).
10. Howarth, M. *et al.* A monovalent streptavidin with a single femtomolar biotin binding site. *Nature Methods* **3,** 267–273 (2006).
11. Alam, S. M. *et al.* Qualitative and quantitative differences in T cell receptor binding of agonist and antagonist ligands. *Immunity* **10,** 227–237 (1999).
12. Rosette, C. *et al.* The impact of duration versus extent of TCR occupancy on T cell activation: a revision of the kinetic proofreading model. *Immunity* **15,** 59–70 (2001).
13. Zhang, F. *et al.* Two-dimensional kinetics regulation of αLβ2-ICAM-1 interaction by conformational changes of the αL-inserted domain. *J. Biol. Chem.* **280,** 42207–42218 (2005).
14. Huang, J. *et al.* Quantifying the effects of molecular orientation and length on two-dimensional receptor-ligand binding kinetics. *J. Biol. Chem.* **279,** 44915–44923 (2004).
15. Mehta, P., Cummings, R. D. & McEver, R. P. Affinity and kinetic analysis of P-selectin binding to P-selectin glycoprotein ligand-1. *J. Biol. Chem.* **273,** 32506–32513 (1998).
16. Wu, L. C., Tuot, D. S., Lyons, D. S., Garcia, K. C. & Davis, M. M. Two-step binding mechanism for T-cell receptor recognition of peptide MHC. *Nature* **418,** 552–556 (2002).
17. Nicholson, M. W., Barclay, A. N., Singer, M. S., Rosen, S. D. & van der Merwe, P. A. Affinity and kinetic analysis of L-selectin (CD62L) binding to glycosylation-dependent cell-adhesion molecule-1. *J. Biol. Chem.* **273,** 763–770 (1998).
18. Zehn, D., Lee, S. Y. & Bevan, M. J. Complete but curtailed T-cell response to very low-affinity antigen. *Nature* **458,** 211–214 (2009).
19. Schamel, W. W. *et al.* Coexistence of multivalent and monovalent TCRs explains high sensitivity and wide range of response. *J. Exp. Med.* **202,** 493–503 (2005).
20. Lillemeier, B. F. *et al.* TCR and Lat are expressed on separate protein islands on T cell membranes and concatenate during activation. *Nature Immunol.* **11,** 90–96 (2009).
21. Campi, G., Varma, R. & Dustin, M. L. Actin and agonist MHC-peptide complex-dependent T cell receptor microclusters as scaffolds for signaling. *J. Exp. Med.* **202,** 1031–1036 (2005).
22. Yokosuka, T. *et al.* Newly generated T cell receptor microclusters initiate and sustain T cell activation by recruitment of Zap70 and SLP-76. *Nature Immunol.* **6,** 1253–1262 (2005).
23. Zidovetzki, R. & Levitan, I. Use of cyclodextrins to manipulate plasma membrane cholesterol content: evidence, misconceptions and control strategies. *Biochim. Biophys. Acta* **1768,** 1311–1324 (2007).
24. Aleksic, M. O. *et al.* Dependence of T cell antigen recognition on T cell receptor-peptide MHC confinement time. *Immunity* **32,** 163–174 (2010).
25. Davis, S. J. & van der Merwe, P. A. The kinetic-segregation model: TCR triggering and beyond. *Nature Immunol.* **7,** 803–809 (2006).
26. McKeithan, T. W. Kinetic proofreading in T-cell receptor signal transduction. *Proc. Natl Acad. Sci. USA* **92,** 5042–5046 (1995).
27. Valitutti, S., Muller, S., Cella, M., Padovan, E. & Lanzavecchia, A. Serial triggering of many T-cell receptors by a few peptide-MHC complexes. *Nature* **375,** 148–151 (1995).

28. Daniels, M. A. *et al.* Thymic selection threshold defined by compartmentalization of Ras/MAPK signalling. *Nature* **444,** 724–729 (2006).
29. Davis, M. M. *et al.* T cells as a self-referential, sensory organ. *Annu. Rev. Immunol.* **25,** 681–695 (2007).
30. Henrickson, S. E. *et al.* T cell sensing of antigen dose governs interactive behavior with dendritic cells and sets a threshold for T cell activation. *Nature Immunol.* **9,** 282–291 (2008).

Supplementary Information is linked to the online version of the paper at www.nature.com/nature.

Acknowledgements We thank the NIH Tetramer Core Facility at Emory University for providing MHC monomers, J. Altman for providing the H-2K^b mutant construct, G. Bao for providing the divalent streptavidin, as well as M. Davis and H.-T. He for commenting on the manuscript. This work was supported by NIH grants AI38282 and AI060799 (to C.Z.) and NS062358, and National Multiple Sclerosis Society Grant RG4047-A-3 (to B.D.E.).

Author Contributions N.J. and C.Z. initiated the research with F5 T cells; J.H. and C.Z. designed the kinetic study; J.H. and B.L. performed the micropipette experiments; V.I.Z. performed the BFP experiments and Monte Carlo simulations; L.J.E. and B.D.E. provided the T cells and conducted the functional study; J.H., V.I.Z., B.L. and C.Z. analysed the data; B.D.E. and C.Z. wrote the paper with all authors contributing.

Author Information Reprints and permissions information is available at www.nature.com/reprints. The authors declare no competing financial interests. Correspondence and requests for materials should be addressed to C.Z. (cheng.zhu@bme.gatech.edu) or B.D.E. (bevavol@emory.edu).

METHODS

Cells and pMHCs. RBCs were isolated from whole blood of healthy volunteers according to protocols approved by the Institutional Review Board of Georgia Institute of Technology. Naive $CD8^+$ OT1 (ref. 7), $CD8^+$ F5 (ref. 7), and $CD4^+$ MOG[31] T cells were generated according to Emory University IACUC approved protocols. Monomeric mouse I-A^b complexed with an MOG peptide (GWYRSPFDRVVH)[31], H-2D^b complexed with an influenza nucleoprotein peptide NP68 (ASNENMDAM)[7], and H-2K^b mutant[9] (constructed by substituting the α3 domain in the mouse H-2K^b with the α3 domain of human HLA-A2) complexed with the following peptides were produced by the NIH Tetramer Core Facility: ovalbumin-derived peptides OVA, A2, G4, E1, V-OVA and R4, and a vesicular stomatitis virus-derived peptide VSV (Table 1)[11,12]. All MHCs have a carboxy-terminal biotin-tag at their α-chain. Monomeric pMHCs were purified by sizing through an S-300 column followed by anion exchange to obtain properly folded molecules. Purified pMHCs were stored at −80 °C and a fresh aliquot was used in each experiment.

Coupling pMHC onto RBCs and beads. Monomeric pMHCs were coated onto RBCs[7] or BFP beads[6] by biotin–streptavidin coupling (Fig. 1c). RBCs were biotinylated using different concentrations (to vary the pMHC density) of biotin-X-NHS (Calbiochem) per manufacturer's instruction[7], incubated with either 1 mg ml^{-1} tetrameric wide-type streptavidin (Pierce) or 0.2 mg ml^{-1} divalent streptavidin[10] for 30 min at 4 °C, and incubated with 20 μg ml^{-1} biotinylated pMHC monomers for 30 min at 4 °C. Cells were washed three times after each step.

For BFP experiments, RBCs were covalently linked with an amine-reactive PEG-biotin polymer (NHS-PEG3400-Biotin, Shearwater Polymers) as previously described[32]. The surfaces of borosilicate beads (2-μm diameter, Duke Scientific) were cleaned in a mixture of ammonium hydroxide and hydrogen peroxide and silanized[32]. Beads were allowed to react with streptavidine-maleimide[6] (Sigma-Aldrich) and incubated with subsaturating concentrations of biotinylated pMHCs for 30 min at room temperature.

Determining molecular densities on the surfaces of T cells, RBCs and beads. Site densities of TCRs on T cells and pMHC on RBCs or beads were measured by flow cytometry (Supplementary Fig. 12). T cells were incubated with a PE-conjugated anti-mouse TCR Vα2 monoclonal antibody B20.1 (BD) at 10 μg ml^{-1} in 200 μl of FACS buffer (RPMI 1640, 5 mM EDTA, 1% BSA and 0.02% sodium azide) at 4 °C for 30 min. Similarly, pMHCs on RBCs/beads were stained with a PE-conjugated anti-mouse H-2K^b (3H2672) (US biological) or a FITC-conjugated anti-mouse H-2D^b (BCDb) monoclonal antibody (Biocarta). T cells or RBCs/beads were analysed by a BD LSR flow cytometer (BD). The fluorescent intensities were compared to standard calibration beads (BD Quantibrite PE Beads, BD or FITC calibration beads, Bangs laboratories) to determine the total number of molecules per cell/bead, which were divided by the cell/bead surface area to obtain site densities[7]. The apparent surface areas of the naive (110 μm^2) and activated (314 μm^2) T cells were calculated as the areas of smooth spheres from their radii measured microscopically. The RBC surface area was taken as 140 μm^2 from ref. 33. The bead surface area was calculated from its 1-μm radius (12.6 μm^2).

Micropipette and BFP apparatuses. As previously described, the micropipette[5,7] (Fig. 1a) and BFP[6,8,34] (Fig. 1b) apparatuses are centred around an inverted microscope placed on an anti-vibration table equipped with manometer systems to apply suction pressures through glass pipettes. Two apposing pipettes are used in both apparatuses to control contacts of a T cell (target) with a pMHC-presenting surface—a RBC (micropipette) or a bead (BFP). The RBC also serves as a force sensor in either case of without (micropipette, Fig. 1a) or with (BFP, Fig. 1b) a bead attaching to its apex. The real-time images are acquired by a CCD camera (30 frames per s) and observed through a TV monitor (micropipette) or display on a computer screen by an image grabber (BFP). In the micropipette apparatus, the two pipettes are respectively mounted on two identical sets of 3D mechanical manipulators for coarse movements and 3D hydraulic manipulators for fine movements. One of the pipettes is also attached to a one-dimensional (1D) piezoelectric translator (PZT) to allow computer-programmed movements for the repeated adhesion test cycles. In the BFP apparatus, the left pipette is mounted on a set of 3D mechanical micrometers for coarse positioning. The right pipette is mounted on a set of 3D PZT for fine positioning and a 1D PZT with capacitive feedback control and subnanometer precision for the adhesion and thermal fluctuation cycles. A third pipette controlled by a pneumatic micromanipulator with a joystick is used to attach a glass bead to the RBC apex to assemble the force probe (Fig. 1b, left). A 24-line strip image across the bead is captured by another high-speed CCD camera (1,500 frames per s, Graftek Imaging) to obtain a well-defined greyscale profile that allows a custom-designed program to track the axial position of the bead with a 5-nm spatial and 0.7-ms temporal resolution, which is displayed in real-time on the computer screen[8] (Supplementary Movie 2). In some experiments, a heater, a humidifier and a thermometer were used to control the temperature at 37 °C.

Adhesion frequency assay. This assay uses micromanipulation to precisely set up cell–cell contact with controlled area/time and uses an ultrasensitive force sensor to mechanically detect the presence of adhesion at the end of the contact. The micropipette apparatus[5] (Fig. 1a) was used for most of the pMHCs because it is simple and easy to use. For pMHCs with off-rates >5 s^{-1}, BFP[6,8] (Fig. 1b) was used because of its higher temporal resolution. Both apparatuses use a pipette to aspirate a T cell and move it in and out of the contact with a pMHC bearing surface. The adhesion sensor in both apparatuses is a pipette-aspirated RBC thanks to its ultrasoft membrane that enables the detection of a subpiconewton force, an order of magnitude smaller than the characteristic force required to break a typical receptor–ligand bond[35], thereby ensuring the detection of single bonds. In the micropipette system, pMHCs are directly coated on the RBC surface and adhesion is detected by visual observation of the RBC membrane deflection (Supplementary Movie 1). In the BFP system, pMHCs are coated on a glass bead attached to the apex of the RBC and adhesion is detected by the bead position deflection with a much higher resolution (Supplementary Movie 2).

The likelihood of adhesion is estimated from the frequency of adhesions occurred in a large number of contacts made under as close to identical conditions as possible. The present work estimated an adhesion frequency P_a from 50 cyclically repeated contacts of a single pair of cells and a mean $P_a \pm$ s.e.m. from several pairs of cells. According to a probabilistic model for adhesion kinetics mediated by a small number bonds[5], the adhesion frequency P_a is related to the average number of bonds $<n>$ by

$$P_a = 1 - \exp(-\langle n \rangle) \quad (1)$$

Assuming a single-step kinetic process of a second-order forward, first-order reverse reaction between monomeric TCR and pMHC molecules, the average number of bonds can be expressed by[5]

$$\langle n \rangle = m_r m_l A_c K_a [1 - \exp(-k_{off} t_c)] \quad (2)$$

where m_r and m_l are respective TCR and pMHC densities, A_c and t_c are contact area and time, and K_a and k_{off} are 2D binding affinity and off-rate. The 2D on-rate can be calculated from $k_{on} = K_a \times k_{off}$.

For each pMHC, >30 pairs of cells were used to obtain several P_a versus t_c curves (for example, Fig. 2a) that corresponded to different TCR and pMHC densities, which were independently measured by flow cytometry. Equations (1) and (2) were fit to each adhesion curve using iterative nonlinear regression to estimate a pair of fitting parameters[36]: the effective 2D affinity A_cK_a and the 2D off-rate k_{off}.

The ability to reliably determine the two model parameters separately is tested by plotting the sum of error squares between the data and the prediction (χ^2) versus the two fitting parameters (Supplementary Fig. 1). The results demonstrate that both model parameters can be identified with good accuracy by fitting the model to the OVA data in Fig. 2c that were measured by a BFP with high temporal resolution. The χ^2 surface (Supplementary Fig. 1b) clearly shows a minimum at $m_r m_l A_c K_a = 0.82$ (Supplementary Fig. 1c, red curve) and $k_{off} = 7.24\ s^{-1}$ (Supplementary Fig. 1d, red curve). By comparison, this is not the case when the same model was fit to the data in Fig. 2a, which are also for OVA but were measured by a micropipette with lower temporal resolution. The χ^2 surface (Supplementary Fig. 1a) has a minimum at $A_cK_a = 0.0002\ \mu m^4$ (Supplementary Fig. 1c, blue curve), indicating the ability to accurately evaluate the effective 2D affinity. However, similarly low χ^2 values are obtained after $k_{off} > 5\ s^{-1}$ (Supplementary Fig. 1d, blue curve). This shows that the off-rate exceeds 5 s^{-1} but its value cannot be determined with accuracy. These results support the use of criterion $k_{off} > 5\ s^{-1}$ for switching from the use of micropipette to BFP for adhesion frequency assay.

Wherever multiple adhesion curves for the same pMHC were measured using different m_r and m_l, the mean and s.e.m. of A_cK_a and k_{off} were calculated from their individual values estimated from fitting each P_a versus t_c curve. Wherever only a single adhesion curve was measured, the s.e.m. values of A_cK_a and k_{off} were generated by the fitting algorithm from the scattering of the P_a data at each contact time[36]. In addition, bootstrapping techniques were used to put 95% confidence intervals on the parameters and the best-fit curves (Fig. 2).

It follows from equation (2) that

$$k_{off} = \ln 2 / t^*_{1/2} \quad (3)$$

where $t^*_{1/2}$ is the time for the average number of bonds $<n>$ to reach half of its maximum value at equilibrium. Because P_a and $<n>$ are related by equation (1), equation (3) translates into

$$k_{off} = \frac{1}{t_{1/2}} \ln \left\{ 1 - \frac{\ln[1 - \frac{1}{2} P_a(\infty)]}{\ln[1 - P_a(\infty)]} \right\}^{-1} \quad (4)$$

where $t_{1/2}$ is the time for the adhesion frequency P_a to reach half of its maximum value at equilibrium $P_a(\infty)$. The criterion of $k_{off} > 5\ s^{-1}$ for switching apparatus

from the micropipette to the BFP is equivalent to that $t^*_{1/2}$ be sufficiently longer than the shortest time (0.05 s) required for the micropipette to reliably detect a residual engagement of the RBC to the T cell on its withdrawal[5].

Unlike the 2D off-rate whose evaluation does not require site densities, the 2D affinity is lumped in equation (2) with the densities of TCR and pMHC. To compensate for the broad 2D affinities range of the TCR for a panel of pMHC ligands of differing potencies, the pMHC densities were adjusted to keep the equilibrium adhesion frequencies in the mid-range using different biotin-X-NHS concentrations to biotinylate the RBCs (for micropipette) or coupling different densities of streptavidin on the probe beads (for BFP). To normalize the effects of site densities, a log transformation is used to convert equations (1) and (2) to equation (5)

$$-\ln(1-P_a)/(m_r m_l) = A_c K_a[1-\exp(-k_{off} t_c)] \quad (5)$$

The applicability of our model to the TCR–pMHC interaction is supported by the data in Supplementary Fig. 2a–f, which collapse distinct adhesion curves measured using different m_r and m_l into a single $-\ln(1-P_a)/(m_r m_l)$ versus t_c curve. It follows from equation (5) that the equilibrium levels of these curves correspond to the $A_c K_a$ values.

From the equilibrium form of equation (5) ($t_c \to \infty$) one obtains

$$-\ln[1-P_a(\infty)] = A_c K_a \cdot m_r m_l \quad (6)$$

a prediction supported by the data in Supplementary Fig. 2g, h, which were obtained using adhesion frequencies measured at 5 s with different site densities. This equation also provides a simple way to measure the $A_c K_a$ from $P_a(\infty)$ without measuring and fitting the entire adhesion curve.

The true or functional contact area A_c depends on the irregular microvillous structure on the T-cell surface[5,37]. It was estimated to be a few per cent of the apparent contact area visualized under the microscope (Supplementary Movies 1 and 2). The apparent contact area was controlled by the computer-programmed PZT movements to be 3 μm^2 (micropipette) and 1 μm^2 (BFP). Because the apparent contact area (and hence the true A_c) was kept constant for all experiments using the same technique (micropipette or BFP), not knowing the precise value for A_c did not affect relative comparisons among affinities of the TCR for different pMHC ligands. Because it is the product of A_c and K_a, and not their separate values, that is returned from fitting data with equations (1) and (2), the results are expressed in terms of $A_c K_a$ (in μm^4), called effective 2D affinity, and of $A_c k_{on}$ (in $\mu m^4 s^{-1}$), called effective 2D on-rate. Because the micropipette and BFP experiments had different true contact areas and because the T cell was contacted by a soft and large membrane in the micropipette experiment but a hard and small bead in the BFP experiment, the $A_c K_a$ and $A_c k_{on}$ values measured by the two techniques were different even for the same TCR–pMHC interaction[37,38]. For consistent comparison among different pMHC ligands, micropipette-measured effective 2D affinities were shown in Figs 3, 4 and Supplementary Figs 2, 4–6 and 8–10, and listed in Table 1. The 2D off-rates presented in these figures and in Table 1 were measured with the micropipette except for the OVA pMHC, which were measured with the BFP. The effective 2D on-rates were calculated by multiplying the effective 2D affinities and off-rates.

Thermal fluctuation assay. This assay was performed using a BFP because of its high resolution and soft spring constant[6]. The spring constant (force required to displace the bead a unit distance by stretching the RBC) was set to be $k_p = 0.15\ pN\ nm^{-1}$ by adjusting the suction pressure Δp according to ref. 39

$$k_p \approx \frac{\pi R_p \Delta p}{(1-R_p/R_0)\ln[4R_0^2/(R_p R_c)]} \quad (7)$$

where R_p, R_0 and R_c are the respective radii of the pipette lumen, the spherical portion of the aspirated RBC, and the contact between the RBC and the bead (Fig. 1b), respectively, which were measured for each force probe assembled. According to the equipartition theorem, the magnitude of the thermal fluctuations, measured by the variance σ^2 of the bead position x, is inversely proportional to the system spring constant k_s

$$\sigma^2 = k_B T/k_s \quad (8)$$

where k_B is the Boltzmann constant and T is absolute temperature. In the absence of any bond between the bead and the T cell, k_s is the same as the force probe spring constant k_p. In the presence of a bond, the force probe is connected to the T cell by another spring k_m. The system spring k_s becomes the sum of k_p and k_m, which reduces the thermal fluctuations according to equation (8). Thus, bond formation and dissociation would produce corresponding reduction and resumption of the thermal fluctuations of the BFP bead (Supplementary Fig. 3 and Supplementary Movie 3). The ensemble standard deviation was approximated by a 70-point sliding standard deviation $\sigma(t)$ of the time course of the force probe position, $x(t)$. This was different from our previous work using beads as a target, which used a 15-point sliding standard deviation[6], because when cells were used, k_m became characteristic of the TCR–pMHC bond and the cell surface structure to which the TCR anchored. The latter structure is very soft, requiring more points to calculate a stable standard deviation. To identify bond association/dissociation events, two thresholds σ_U (black dashed line) and σ_L (red solid line) were set in the $\sigma(t)$ versus t plot (horizontal lines, Supplementary Fig. 3b). The time when $\sigma(t)$ crossed σ_L from above identifies the instant of bond association, and the time $\sigma(t)$ crossed σ_U from below identifies the instant of bond dissociation (Supplementary Fig. 3, red arrow).

Bond lifetime t_b can be measured from the instant of bond association to the instant of bond dissociation. Modelling the kinetic process as a single-step first-order dissociation of a single monomeric TCR–pMHC bond, the probability P_b of a bond formed at time 0 to remain intact at time t_b is

$$P_b = \exp(-k_{off} t_b) \quad (9)$$

Taking a natural log linearizes the exponential function on right hand-side of equation (9). We thus plot the bond lifetime data as ln(Number of events with a life time $\geq t_b$) versus t_b to estimate the off-rate k_{off} from the negative slope of the line (Fig. 2d).

Monte Carlo simulations. Monte Carlo simulations of the adhesion frequency assay assumed 40 pMHCs randomly placed in a square contact area of 4 μm^2 with periodic boundary conditions, which can diffuse ($D = 0.15\ \mu m^2 s^{-1}$) and form bonds with 600 TCRs that were either evenly distributed or organized as 20 clusters of 5×6 TCRs each with 10 nm spacing between molecules. Simulation began with unbound state for all pMHCs. The two cells were placed into contact of a specified duration. During the contact a free TCR and a free pMHC could form a bond with a given probability (below). Any bond could dissociate with a probability P_d (0.05). A contact was said to produce an adhesion if there were any bonds at the end of the contact duration; otherwise no adhesion was produced. Each contact was followed by a period of cell separation (0.5 s), during which the molecules continued to diffuse but did not interact. This contact–separation cycle was repeated 50 times for each cell pair. Five cell pairs were simulated for each contact duration, ranging from 0.01 to 5 s. Two different models for the binding probability were assumed: (1) the same probability P_{assoc} (0.02) for forming a TCR–pMHC bond whenever the two molecules come closer than a specified reaction radius (10 nm), and (2) P_{assoc} for forming a TCR–pMHC bond if no TCR in a cluster binds a pMHC in the past time step Δt (0.005 s), but $P_{assoc} \times k$ for all the TCR molecules in the cluster if one of them has previously interacted with a pMHC in the past time step. Here k (5) is an amplification factor. This is to simulate a form of cooperative binding such that, each time the pMHC binds a TCR, all TCRs of the same cluster acquire an increased ability to bind pMHC. The first model was tested for both evenly distributed and clustered TCR cases. The second model was used for clustered TCR only.

Pharmacological treatments. Cells in the micropipette and BFP experiments were suspended in a chamber filled with L-15 medium (Sigma-Aldrich) plus 5 mM HEPES and 1% BSA. In some experiments, T cells were incubated with methyl-β-cyclodextrin (MβCD, Sigma-Aldrich), cholesterol oxidase (CO, Sigma-Aldrich) or latrunculin A (LA, Calbiochem) at a given concentration for 1 h at 37 °C (MβCD and CO) or for 30 min at 25 °C (LA) before adding to the chamber. Adhesion frequency assays were performed in the absence (MβCD) or continuous presence (CO or LA) of the same concentration of the pharmacological agent[7].

31. Sabatino, J. J. Jr, Shires, J., Altman, J. D., Ford, M. L. & Evavold, B. D. Loss of IFN-γ enables the expansion of autoreactive $CD4^+$ T cells to induce experimental autoimmune encephalomyelitis by a nonencephalitogenic myelin variant antigen. *J. Immunol.* **180,** 4451–4457 (2008).
32. Evans, E., Leung, A., Heinrich, V. & Zhu, C. Mechanical switching and coupling between two dissociation pathways in a P-selectin adhesion bond. *Proc. Natl Acad. Sci. USA* **101,** 11281–11286 (2004).
33. Hochmuth, R. M. in *Handbook of Bioengineering* (eds Skalak, R. & Chien, S.) (McGraw-Hill, 1987).
34. Lou, J. *et al.* Flow-enhanced adhesion regulated by a selectin interdomain hinge. *J. Cell Biol.* **174,** 1107–1117 (2006).
35. Zhu, C., Long, M. & Bongrand, P. Measuring receptor/ligand interaction at the single bond level: experimental and interpretive issues. *Ann. Biomed. Eng.* **30,** 305–314 (2002).
36. Williams, T. E., Selvaraj, P. & Zhu, C. Concurrent binding to multiple ligands: kinetic rates of CD16b for membrane-bound IgG1 and IgG2. *Biophys. J.* **79,** 1858–1866 (2000).
37. Williams, T. E., Nagarajan, S., Selvaraj, P. & Zhu, C. Quantifying the impact of membrane microtopology on effective two-dimensional affinity. *J. Biol. Chem.* **276,** 13283–13288 (2001).
38. Wu, L. *et al.* Impact of carrier stiffness and microtopology on two-dimensional kinetics of P-selectin and P-selectin glycoprotein ligand-1 (PSGL-1) interactions. *J. Biol. Chem.* **282,** 9846–9854 (2007).
39. Evans, E., Heinrich, V., Leung, A. & Kinoshita, K. Nano- to microscale dynamics of P-selectin detachment from leukocyte interfaces. I. Membrane separation from the cytoskeleton. *Biophys. J.* **88,** 2288–2298 (2005).

ERRATUM

doi:10.1038/nature08944

The kinetics of two-dimensional TCR and pMHC interactions determine T-cell responsiveness

Jun Huang, Veronika I. Zarnitsyna, Baoyu Liu, Lindsay J. Edwards, Ning Jiang, Brian D. Evavold & Cheng Zhu

Nature **464**, 932–936 (2010).

In three places in the 'Monte Carlo simulations' section of the online-only Methods of this Letter, the association probability P_a should have been denoted P_{assoc} to distinguish it from the adhesion probability P_a.